

Precision measurement of electron affinity of Zr and fine structures of its negative ions

Xiaoxi Fu, Jiaming Li, Zhihong Luo, Xiaolin Chen, and Chuangang Ning

Citation: [The Journal of Chemical Physics](#) **147**, 064306 (2017);

View online: <https://doi.org/10.1063/1.4986547>

View Table of Contents: <http://aip.scitation.org/toc/jcp/147/6>

Published by the [American Institute of Physics](#)

Articles you may be interested in

[Accurate electron affinity of V and fine-structure splittings of \$V^-\$ via slow-electron velocity-map imaging](#)
The Journal of Chemical Physics **145**, 164307 (2016); 10.1063/1.4965928

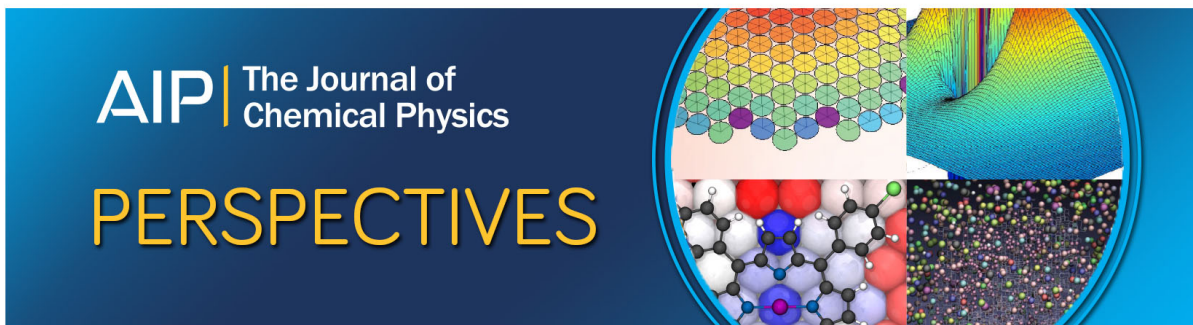
[A multi-plate velocity-map imaging design for high-resolution photoelectron spectroscopy](#)
The Journal of Chemical Physics **147**, 094201 (2017); 10.1063/1.4996011

[Perspective: Advanced particle imaging](#)
The Journal of Chemical Physics **147**, 013601 (2017); 10.1063/1.4983623

[The collision-free photochemistry of methyl azide at 157 nm: Mechanism and energy release](#)
The Journal of Chemical Physics **147**, 064307 (2017); 10.1063/1.4997783

[Binding energies of hydrated cobalt hydroxide ion complexes: A guided ion beam and theoretical investigation](#)
The Journal of Chemical Physics **147**, 064305 (2017); 10.1063/1.4991557

[Accurate electron affinity of Pb and isotope shifts of binding energies of \$Pb^-\$](#)
The Journal of Chemical Physics **145**, 084303 (2016); 10.1063/1.4961654



Precision measurement of electron affinity of Zr and fine structures of its negative ions

Xiaoxi Fu,¹ Jiaming Li,¹ Zhihong Luo,¹ Xiaolin Chen,¹ and Chuangang Ning^{1,2,a)}

¹Department of Physics, State Key Laboratory of Low-Dimensional Quantum Physics, Tsinghua University, Beijing 10084, China

²Collaborative Innovation Center of Quantum Matter, Beijing, China

(Received 5 June 2017; accepted 26 July 2017; published online 11 August 2017)

The high-resolution photoelectron spectra of Zr^- were obtained via the slow-electron velocity-map imaging method. The electron affinity of Zr was measured to be $3494.67(72) \text{ cm}^{-1}$ or $0.433\ 283(89) \text{ eV}$. The accuracy has been improved by a factor of 160 compared with the previous result. The fine structures of Zr^- were also well resolved: $251.0(37)$ (${}^4F_{5/2}$), $579.6(8)$ (${}^4F_{7/2}$), and $971.7(12) \text{ cm}^{-1}$ (${}^4F_{9/2}$) above the ground state ${}^4F_{3/2}$. Published by AIP Publishing. [<http://dx.doi.org/10.1063/1.4986547>]

I. INTRODUCTION

Electron affinity (EA) is referred to as the energy difference between a neutral atom or a molecule and its negative ion at their ground states. It is used to describe the ability of an atom or a molecule to accept an electron. Negative ions, or anions, are unique species and are also chemically important. Their electronic structures and properties are generally different from those of neutral atoms and positive ions. In addition to the regime of gas-phase ion chemistry, areas such as interstellar chemistry^{1,2} and molecular clusters^{3,4} have witnessed the utility of EAs. Moreover, studies of the stabilities of free radicals and anions can provide an insight into electron transfer in biological systems,^{5–7} photosynthesis,^{8–10} and toxin chemistry.¹¹ Consequently, numerous attempts have been made to improve the accuracy of the experimental EA values as well as the theoretical ones.

Thus far, there have been four main experimental techniques used to measure EAs. A majority of EA values of transition metals were measured via the generic laser photoelectron spectroscopy (LPES) method by Lineberger and co-workers in 1981.¹² However, the limited energy resolution of LPES around 10 meV has impeded the improvement of the accuracy of EAs.^{12–15} Another method named the laser photodetachment threshold (LPT) method depends on the Wigner threshold law,¹⁶ which predicts that the photodetachment cross section σ is proportional to $(E_k)^{l+1/2}$. Here, l is the angular quantum number of the outgoing photoelectron after the detachment, and E_k is its kinetic energy. Apparently, this method provides a straightforward probe of EA values for an s -wave detachment due to the sharp onset of the cross section near the threshold. However, it becomes unreliable for a p -wave detachment due to the zero-slope onset. Moreover, this method fails to resolve the congested p -wave detachment channels that are common for transition elements because of their unique electronic configurations. As a result, the LPT method is more applicable to the EA measurement of the main group elements than the transition metals.^{17–19} The uncertainty of EAs for the

most transition elements still remains around 10 meV although many efforts have been directed toward the improved accuracy over the past half century.²⁰ Only a few EA values of the late transition metals were measured using LPT method, such as Ni and Pd.²¹ Recently, Blondel and co-workers introduced the laser photodetachment microscopy (LPM) method. The uncertainties of O and C have been successfully reduced down to sub- μeV level with the LPM method.^{22,23} However, the kinetic energy of the outgoing photoelectron is restricted to be lower than 1 cm^{-1} otherwise it cannot be derived via the interference patterns. The count rate of p -wave photodetachment will become impractically low at such a low kinetic energy. Therefore, the LPM method is not applied for transition metals either. Fortunately, the slow-electron velocity-map imaging (SEVI) technique manages to improve the energy resolution of low-energy electrons to a few cm^{-1} while maintaining the signal intensity to an acceptable level.^{24–29} The reason lies in that it generally measures the photoelectron with E_k around 100 cm^{-1} . Therefore, the signal intensity is much higher than that just above the photodetachment threshold. Neumark and co-workers have demonstrated the features of this method in the high resolution of photoelectron spectroscopy of molecular anions.^{30,31}

In our previous work, we have reported the EA values with high accuracy of some transition metals using the SEVI method.^{29,32–36} In this paper, we employed this method to measure the EA value of zirconium (Zr) and the fine-structure splittings of Zr^- . Zirconium is mainly used as a refractory and an opacifier. Because of its chemical resistance, zircon is also used in aggressive environments, such as moulds for molten metals. The ground-state configuration of Zr^- is $(4d^35s^2)\ {}^4F_{3/2}$, while the ground-state configuration of Zr is $(4d^25s^2)\ {}^3F_2$. Lineberger and co-workers reported the EA value of Zr to be $0.427(14) \text{ eV}$ with the LPES method.¹²

II. EXPERIMENTAL SETUP

The experiment was conducted using a slow-electron velocity-map imaging apparatus equipped with a laser ablation

^{a)}Electronic mail: ningcg@tsinghua.edu.cn

ion source. This apparatus has been described in detail previously.³⁴ In brief, it can be roughly divided into three parts: a laser ablation ion source, a Wiley-McLaren type time-of-flight (TOF) mass spectrometer, and a photoelectron velocity-map-imaging (VMI) system. The negative ions Zr^- are generated in the ion source by focusing a pulsed laser onto a continually rotating and translating Zr metal disk. The ablation laser is the second-harmonic output of a Nd: YAG laser (532 nm) (20 Hz, ~ 15 mJ/pulse). In view of the fact that transition metals are easily oxidized, an in-line sodium oven releasing sodium vapor is helpful to remove the contamination consisting of trace oxygen and water. Otherwise, the zirconium oxide species are dominant in the mass spectrum. After the skimmer, the anions are extracted perpendicularly into a TOF mass spectrometer. The anionic species are accelerated to 900 eV by a high-voltage pulse and then are guided by a set of deflectors and focused by a set of Einzel lenses into a 1.4-m-long TOF tube. The mass resolution $M/\Delta M$ of the current design is 300 for $M \sim 100$. Then the target ions are selected by the mass gate and detected by an in-line microchannel plate detector. This rotatable ion detector is supposed to be moved out of the ion path so that the target ions can be overlapped with the detachment laser beam after entering the VMI lens system. The detachment laser beam is limited to 3 mm in diameter by passing through a series of apertures. Finally, the detached photoelectrons are projected onto a phosphor screen behind a set of microchannel plates and recorded by a CCD camera. A real-time intensity-weighted centroid program is applied to reconstruct the position of each photoelectron. Typically, each photoelectron imaging is an accumulated result of 50 000–200 000 laser shots. The photodetachment laser is from a Spectra-physics dye laser system (400–920 nm, linewidth 0.06 cm⁻¹ at 625 nm) pumped by a Quanta-Ray Pro 290 Nd: YAG laser (20 Hz, 1000 mJ/pulse at 1064 nm). The photon energy ($h\nu$) is further measured by a HighFinesse WS6-600 wavelength meter with an accuracy of 0.02 cm⁻¹. The photoelectron spectrum was reconstructed from the accumulated image using the maximum entropy velocity Legendre reconstruction (MEVELER) method.³⁵

III. RESULTS AND DISCUSSION

Figure 1 shows the photoelectron images and binding energy spectra obtained at photon energies of $h\nu = 14\,910.71$, $15\,032.08$, and $15\,680.64$ cm⁻¹, respectively. The imaging voltage is -150 V. According to the selection rules, there are six allowed transitions between Zr^- (4F) and Zr (3F), which are labeled as $a-f$ in Fig. 1. This assignment was made based on the calculated energy levels of Zr^- and the standard atomic levels of Zr . The diagram of the transitions is illustrated in Fig. 2. There are five peaks in Fig. 1(c). The first broad peak consists of three transitions a , b , and c according to the theoretical simulations. Peak d belongs to the transition Zr (3F_2) $\leftarrow Zr^-$ ($^4F_{3/2}$), which is the only channel originating from the ground state of Zr^- . Therefore, the transition Zr (3F_2) $\leftarrow Zr^-$ ($^4F_{3/2}$) is selected as the channel to measure the EA value in this work. Peaks e and f represent the transitions Zr (3F_3) $\leftarrow Zr^-$ ($^4F_{5/2}$) and Zr (3F_4) $\leftarrow Zr^-$ ($^4F_{7/2}$), respectively. Since the energy levels of Zr (3F_2), Zr (3F_3), and Zr (3F_4) are

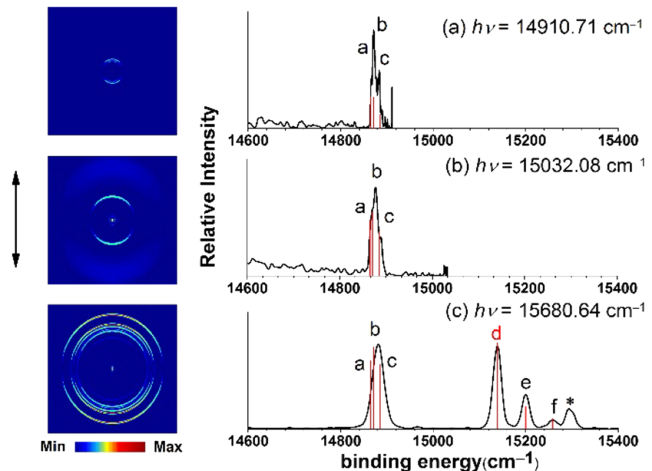


FIG. 1. Photoelectron images and spectra of Zr^- ions at photon energies of $14\,910.71$ cm⁻¹ (a), $15\,032.08$ cm⁻¹ (b), and $15\,680.64$ cm⁻¹ (c). The double arrow indicates the laser polarization. The red sticks are the theoretical simulations at the ion temperature of 800 K. Peak d is related to the Zr (3F_2) $\leftarrow Zr^-$ ($^4F_{3/2}$) transition, which is used to measure the electron affinity of Zr in this present work. The peak labeled with asterisk (*) is due to an unknown contamination.

accurately known from the NIST database,³⁸ the energy gap between any two levels among Zr^- ($^4F_{3/2}$), Zr^- ($^4F_{5/2}$), and Zr^- ($^4F_{7/2}$) can be derived from peaks d , e , and f . In addition, the binding energy of transitions b and c can also be extracted from peaks e and f . The peak labeled with asterisk (*) is due to an unknown contamination. In order to determine the energy level of Zr^- ($^4F_{9/2}$), we need a better energy resolution to resolve transition a . One of the important advantages of SEVI is that its energy resolution can be improved by lowering the kinetic energy of photoelectrons. As shown in Fig. 1(a), peaks a , b , and c can be partly resolved at a lower photon energy of $14\,910.71$ cm⁻¹. The Gaussian function fitting procedure was used to obtain the binding energy of transition a . Once the binding energy of transition a is known, the energy level of Zr^- ($^4F_{9/2}$) is determined. The binding energies of all peaks and the energy levels of all related states are summarized in Table I. The relatively large uncertainty of the binding energy of peak c is mostly attributed to the statistical fluctuations due to the very

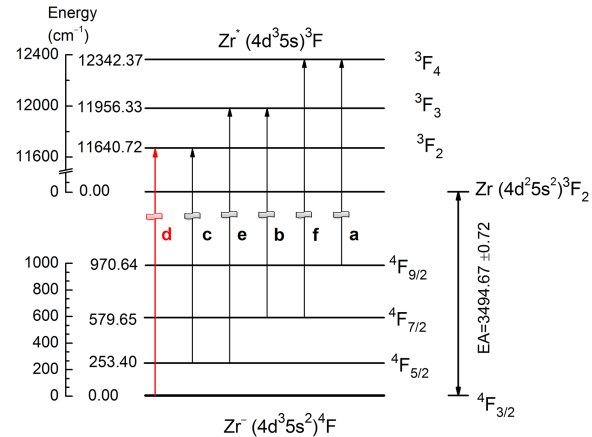


FIG. 2. Energy levels of Zr and Zr^- related to the present measurement. The ground state of Zr is $(4d^25s^2)^3F_2$. The ground state of Zr^- is $(4d^35s^2)^4F_{3/2}$. The labels of each transition are the indices of the observed peaks in Fig. 1. Transition d is used for the electron affinity measurement.

TABLE I. Measured binding energies and fine structures of Zr^- and the electron affinity of Zr.

Peaks	Levels ($Zr \leftarrow Zr^-$)	Binding energy (cm^{-1})
<i>a</i>	$^3F_4 \leftarrow ^4F_{9/2}$	14 865.34(95)
<i>b</i>	$^3F_3 \leftarrow ^4F_{7/2}$	14 871.4(3)
<i>c</i>	$^3F_2 \leftarrow ^4F_{5/2}$	14 884.4(36)
<i>d</i>	$^3F_2 \leftarrow ^4F_{3/2}$	15 135.39(72)^a
<i>e</i>	$^3F_3 \leftarrow ^4F_{5/2}$	15 200.0(36)
<i>f</i>	$^3F_4 \leftarrow ^4F_{7/2}$	15 259.0(34)
Fine structures of Zr^- (cm^{-1})		
Levels	Extrapolated ¹²	Experimental
$^4F_{5/2} \leftarrow ^4F_{3/2}$	250(50)	251.0(37)
$^4F_{7/2} \leftarrow ^4F_{3/2}$	580(86)	579.6(8)
$^4F_{9/2} \leftarrow ^4F_{3/2}$	950(100)	971.7(12)
Electron affinity of Zr		
Value	Reference	
0.343 eV	Rakhлина <i>et al.</i> ⁴⁰ (calculated)	
0.427(14) eV	Feigerle <i>et al.</i> ¹² (measured)	
0.433 283(89) eV or	This work (measured)	
3494.67(72) cm^{-1}		

^aInformation in bold signifies the selected channel for EA measurement.

low count rate. The red sticks in Fig. 1 represent the calculated intensity at the ion temperature of 800 K. The calculated intensity has been rescaled according to Wigner's law $\sigma \propto (E_k)^{3/2}$ for p -wave detachment. It can be seen that the simulation agrees well with the experimental spectra.

To accurately determine the electron affinity of Zr, transition *d* [$Zr(^3F_2) \leftarrow Zr^-(^4F_{3/2})$] was further scanned around its threshold. A fine energy calibration of the VMI system for peak *d* was conducted by changing the photon energy from 15 171 cm^{-1} to 15 211 cm^{-1} with a $\sim 10 \text{ cm}^{-1}$ step. The radius can be obtained by performing the Gaussian function fitting. The measured r^2 versus the photon energy $h\nu$ is plotted in Fig. 3. The energy calibration parameters of the linear relation between $h\nu$ and r^2 were determined by least squares fitting. The binding energy of transition *d* and its uncertainty were also obtained by this procedure. Figure 4 shows the measured

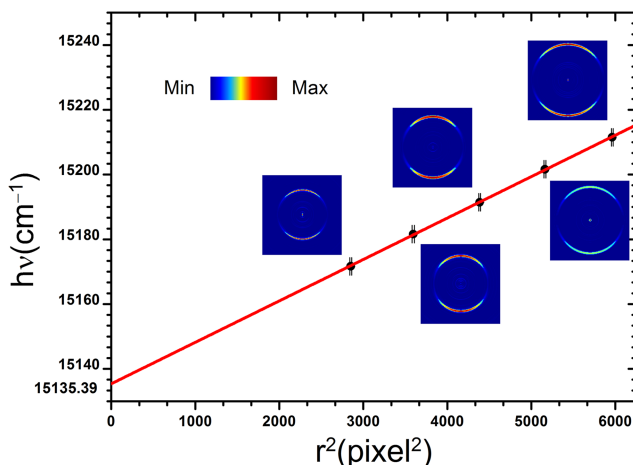


FIG. 3. Energy calibration of the photoelectron velocity-map imaging system. Points with error bars are experimental data of transition *d*. The solid line is the linear least squares fitting. The intercept 15 135.39 cm^{-1} is the binding energy of transition *d*. The rings above each point are the photoelectron images.

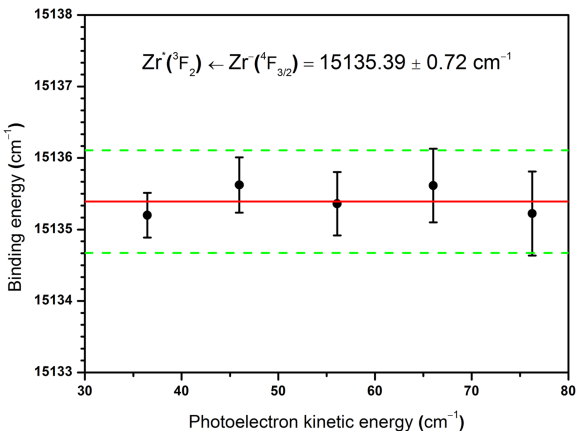


FIG. 4. Binding energy of $Zr(^3F_2) \leftarrow Zr^-(^4F_{3/2})$ transition measured as a function of the kinetic energy of photoelectrons. The dotted lines indicate the $\pm 0.72 \text{ cm}^{-1}$ uncertainty.

binding energy versus the kinetic energy of photoelectrons. Its mean binding energy is 15 135.39 cm^{-1} with an uncertainty of 0.72 cm^{-1} . The uncertainty of 0.72 cm^{-1} included the contribution of the laser linewidth 0.06 cm^{-1} . The energy level of the neutral Zr atom ($4d^3 5s$) 3F_2 is 11 640.72 cm^{-1} above its ground state. Subtracting 11 640.72 cm^{-1} from the binding energy 15 135.39 cm^{-1} yields the EA value of Zr: 3494.67(72) cm^{-1} or 0.433 283(89) eV, which is consistent with the previously reported value of 0.427(14) eV.¹² The accuracy is improved by a factor of 160. Note that 1 eV = 8065.544 005(50) cm^{-1} , as recommended by 2014 CODATA.³⁹ The fine-structure splittings of Zr^- are determined to be 251.0(37) ($^4F_{5/2}$), 579.6(8) ($^4F_{7/2}$), and 971.7(12) ($^4F_{9/2}$) cm^{-1} above the ground state $^4F_{3/2}$. In Table I, the previous extrapolated values of the splittings 250(50), 580(86), and 950(100) cm^{-1} are also listed for comparison.¹² As can be seen, the extrapolated values agree with our measurement very well. As for the theoretical side, Rakhлина *et al.* combined the superposition of configurations and the determinant perturbation theory to calculate the EA value of Zr to be 0.343 eV.⁴⁰

IV. CONCLUSIONS

In conclusion, the electron affinity of Zr was measured to be 3494.67(72) cm^{-1} or 0.433 283(89) eV via the slow electron velocity imaging method. The accuracy was improved by a factor of 160 compared with the previous measurement. The fine structures of Zr^- were also successfully resolved. The accurate value of the electron affinity of Zr and the fine-structure splittings of Zr^- determined in this study could serve as a benchmark for developing more accurate theoretical methods for transition metals.

ACKNOWLEDGMENTS

This work is supported by the National Natural Science Foundation of China (NSFC) (Grant Nos. 91336104 and 11504198).

¹J. P. Maier, *J. Phys. Chem. A* **102**, 3462 (1998).

²D. M. Hudgins and L. J. Allamandola, *J. Phys. Chem.* **99**, 8978 (1995).

³K. R. Asmis, T. R. Taylor, and D. M. Neumark, *Chem. Phys. Lett.* **308**, 347 (1999).

- ⁴B. J. Greenblatt, M. T. Zanni, and D. M. Neumark, *Science* **276**, 1675 (1997).
- ⁵H. Han and M. B. Zimmt, *J. Am. Chem. Soc.* **120**, 8001 (1998).
- ⁶S. P. Greatbanks, J. E. Gready, A. C. Limaye, and A. P. Rendell, *Proteins: Struct., Funct., Genet.* **37**, 157 (1999).
- ⁷S. P. Greatbanks, J. E. Gready, A. C. Limaye, and A. P. Rendell, *J. Comput. Chem.* **21**, 788 (2000).
- ⁸M. G. Cory and M. C. Zerner, *J. Am. Chem. Soc.* **118**, 4148 (1996).
- ⁹M. Nonella, *Photosynth. Res.* **55**, 253 (1998).
- ¹⁰J. Crystal and R. A. Friesner, *J. Phys. Chem. A* **104**, 2362 (2000).
- ¹¹S. Arulmozhiraja, T. Fujii, and H. J. Tokiwa, *Phys. Chem. A* **104**, 7068 (2000).
- ¹²C. S. Feigerle, R. R. Corderman, S. V. Bobashev, and W. C. Lineberger, *J. Chem. Phys.* **74**, 1580 (1981).
- ¹³V. T. Davis, J. Thompson, and A. Covington, *Nucl. Instrum. Methods Phys. Res., Sect. B* **241**, 118 (2005).
- ¹⁴J. Felton, M. Ray, and C. C. Jarrold, *Phys. Rev. A* **89**, 033407 (2014).
- ¹⁵D. G. Leopold and W. C. Lineberger, *J. Chem. Phys.* **85**, 51 (1986).
- ¹⁶E. P. Wigner, *Phys. Rev.* **73**, 1002 (1948).
- ¹⁷D. M. Neumark, K. R. Lykke, T. Andersen, and W. C. Lineberger, *Phys. Rev. A* **32**, 1890 (1985).
- ¹⁸M. Scheer, R. C. Bilodeau, and H. K. Haugen, *Phys. Rev. Lett.* **80**, 2562 (1998).
- ¹⁹M. Scheer, R. C. Bilodeau, C. A. Brodie, and H. K. Haugen, *Phys. Rev. A* **58**, 2844 (1998).
- ²⁰H. Hotop and W. C. Lineberger, *J. Phys. Chem. Ref. Data* **14**, 731 (1985).
- ²¹M. Scheer, C. A. Brodie, R. C. Bilodeau, and H. K. Haugen, *Phys. Rev. A* **58**, 2051 (1998).
- ²²C. Blondel, C. Delsart, C. Valli, S. Yiou, M. R. Godefroid, and S. Van Eck, *Phys. Rev. A* **64**, 052504 (2001).
- ²³D. Bresteanu, C. Drag, and C. Blondel, *Phys. Rev. A* **93**, 013414 (2016).
- ²⁴J. B. Kim, J. A. DeVine, D. S. Levine, and D. M. Neumark, *J. Am. Chem. Soc.* **137**, 1420 (2015).
- ²⁵J. B. Kim, M. L. Weichman, T. F. Sjorlander, D. M. Neumark, J. Klos, M. H. Alexander, and D. E. Manolopoulos, *Science* **349**, 510 (2015).
- ²⁶H. T. Liu, C. G. Ning, D. L. Huang, P. D. Dau, and L. S. Wang, *Angew. Chem., Int. Ed.* **53**, 2464 (2014).
- ²⁷H. T. Liu, C. G. Ning, D. L. Huang, and L. S. Wang, *Angew. Chem., Int. Ed.* **52**, 8976 (2013).
- ²⁸I. Leon, Z. Yang, H. T. Liu, and L. S. Wang, *Rev. Sci. Instrum.* **85**, 083106 (2014).
- ²⁹X. L. Chen and C. G. Ning, *J. Chem. Phys.* **145**, 084303 (2016).
- ³⁰A. Osterwalder, M. J. Nee, J. Zhou, and D. M. Neumark, *J. Chem. Phys.* **121**, 6317 (2004).
- ³¹D. M. Neumark, *J. Phys. Chem. A* **112**, 13287 (2008).
- ³²X. L. Chen, Z. H. Luo, J. M. Li, and C. G. Ning, *Sci. Rep.* **6**, 24996 (2016).
- ³³X. L. Chen and C. G. Ning, *Phys. Rev. A* **93**, 052508 (2016).
- ³⁴Z. H. Luo, X. L. Chen, J. M. Li, and C. G. Ning, *Phys. Rev. A* **93**, 020501 (2016).
- ³⁵X. X. Fu, Z. H. Luo, X. L. Chen, J. M. Li, and C. G. Ning, *J. Chem. Phys.* **145**, 164307 (2016).
- ³⁶X. L. Chen and C. G. Ning, *J. Phys. Chem. Lett.* **8**, 2735 (2017).
- ³⁷B. Dick, *Phys. Chem. Chem. Phys.* **16**, 570 (2014).
- ³⁸J. E. Sansonetti and W. C. Martin, *J. Phys. Chem. Ref. Data* **34**, 1559 (2005).
- ³⁹P. J. Mohr, D. B. Newell, and B. N. Taylor, *Rev. Mod. Phys.* **88**, 035009 (2016).
- ⁴⁰Yu. G. Rakhlina, M. G. Kozlov, and S. G. Porsev, *Opt. Spectrosc.* **90**, 817 (2001).